ADVANCED INTELLIGENT SYSTEMS
Open Access
www.advintellsyst.com

Electronic Contact Lens: A Platform for Wireless Health Monitoring Applications

*Mengyao Yuan, Rupam Das, Rami Ghannam, Yinhao Wang, Julien Reboud, Roland Fromme, Farshad Moradi, and Hadi Heidari**

Electronic contact lenses are used for noninvasively monitoring vital human signs and medical parameters. However, maintaining a secure communications connection and a self-sustainable power source are still looming challenges. Herein, a proof-of-concept electronic contact lens is demonstrated that includes a spiral antenna with its wireless circuit unit for data telemetry, a rectifier circuit for power conditioning, and a micro-light-emitting diode (μLED) as a load. The spiral antenna with its rectifying circuit is designed considering operation in the industrial, scientific, and medical (ISM) band of 2.4 GHz. The spiral coil with an inner diameter of 10 mm, an outer diameter of 12 mm, and a wire width of 0.2 mm is fabricated on a donut-shaped flexible polyimide substrate. For biocompatibility purposes, polyimide is used as the contact lens substrate and polydimethylsiloxane (PDMS) is used for encapsulation. A 3D-printed eye model is developed for accurately shaping the curvature of the PDMS-encapsulated contact lens. The reflection coefficient (S_{11}) of the fabricated antenna is tested in different conditions and on an eye model to mimic the liquid condition of the human eye. In a wide range of conditions, a minimum of −20 dB reflection coefficient (S_{11}) is obtained.

1. Introduction

Traditionally, contact lenses have been used for treating vision impairments such as myopia, hyperopia, and astigmatism. More recently, electronic contact lenses have been considered as an effective noninvasive platform for detecting and diagnosing vital human signs, particularly for the detection of glucose levels in diabetic patients, as well as glaucoma.[1–5] Thanks to the integration of biotechnology, information technology, and microelectronics on the contact lens platform, various biosensors and electrochemical sensors have been developed on lenses for the detection of these biomarkers.[6] They have also been considered for protecting eyes from electromagnetic waves and dehydration, thereby reducing the risk of cataracts.[7,8] These electronic lenses integrate microelectronics on a soft or hard substrate for different sensing purposes.

To ensure uninterrupted operation, energy supply to the electronic contact lens needs careful consideration. For example, Nasreldin et al. have investigated the use of flexible batteries that are integrated on the lenses.[9] However, battery lifetime and replacement become an issue. Thus, scavenging energy using piezoelectric sensors has been proposed[10] but is yet to be fully investigated in the literature. Consequently, wireless energy harvesting has been considered as an effective approach for contact lenses.[1,10,11] Such electronic contact lenses[12] contain a power transfer unit, a read-out circuit (including the disease-diagnosing sensor), and encapsulation to avoid direct contact between the electronic devices and the human eye. Such lenses were designed for testing blood glucose using tears. With this noninvasive method, the pain associated with traditional fingertip blood tests can be reduced and blood sugar levels can always be monitored. However, there is no efficient system for simultaneously powering and communicating the detected information on the lens.

In comparison with other energy-harvesting methods, wireless power transfer (WPT) prevents damage to human tissue and eliminates the risk of infection, as there are no wires running through the skin or other autologous tissues.[13–18] As a

M. Yuan, Dr. R. Das, Dr. R. Ghannam, Y. Wang, Dr. J. Reboud, Dr. H. Heidari
James Watt School of Engineering
University of Glasgow
Glasgow G12 8QQ, UK
E-mail: hadi.heidari@glasgow.ac.uk

The ORCID identification number(s) for the author(s) of this article can be found under https://doi.org/10.1002/aisy.201900190.

DOI: 10.1002/aisy.201900190

R. Fromme
Chemical Engineering
Wöhlk Contactlinsen GmbH
D-24232 Schönkirchen, Germany

Dr. F. Moradi
Department of Engineering
Aarhus University
8200 Aarhus, Denmark

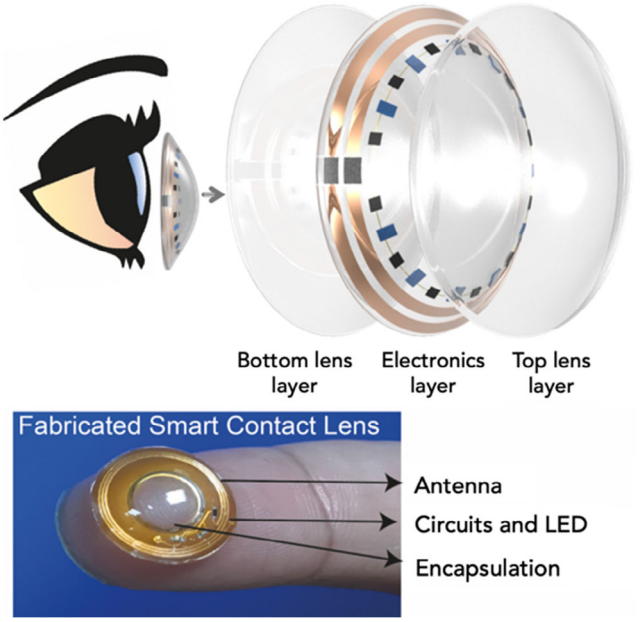

Figure 1. A conceptual schematic and fabricated version of the developed electronic contact lens.

nonradiative method, WPT is based on inductive power transfer between coils, where energy is transmitted through magnetic fields. Moreover, the WPT transmitter output power is constrained to 0.5–2 W for smart contact lenses, which satisfies U.S. Food and Drug Administration (FDA) regulations regarding the safe amount of power transfer without increasing tissue temperature.[19]

Moreover, antenna design in electronic contact lenses is very important. Previous designs that relied on a serpentine structure[9] for power transfer and communications might impede eyesight, since the eyeball's physical structure is not carefully considered. Therefore, our design was based on a spiral coil antenna, which was fabricated on a polyimide flexible substrate and encapsulated with polydimethylsiloxane (PDMS).[20] Because antenna performance is affected by the proximity of other electronic components, the fabricated stretchable coil was tested in the presence of electronic circuits, which include the rectifier and the micro-light-emitting diode (μLED) (**Figure 1**). Our experimental results were compared with finite element simulations. In addition, the performance of the fabricated contact lens was tested under various conditions that imitate a real eye environment.

This article is organized as follows. Section 2 provides an overview of the state of the art in wireless electronic contact lenses. Section 3 introduces our methodology. Section 4 provides our fabrication process. The experimental and simulation results of the antenna *S*-parameters are presented in Section 5. Finally, concluding remarks are provided in Section 6.

2. Recent Advances in Electronic Contact Lenses

Advances in nanotechnology have made it technically feasible to put together electronic devices such as sensors, transmitters, amplifiers, and even displays within the confines of standard-size contact lenses.[21–25] Delivering small amounts of power to these electronic components in a contact lens is a challenge. However, we believe that WPT technology can help achieve this goal.

WPT technology can be divided into inductively coupled power transfer (ICPT), ultrasonic power transfer (UPT), and capacitively coupled power transfer (CCPT), which have all been used for powering various electronic devices on the human body. However, CCPT requires a capacitor and UPT needs an energy generator on the receiver side. Thus, both these technologies will add unnecessary thickness to our electronic contact lens, which will cause discomfort for the wearer. Thus, the simple design and high efficiency of ICPT (>20%) make it ideal for implantable biomedical application,[26,27] especially for electronic contact lenses.[28–33]

ICPT is a technology that relies on power transformation through a magnetic field generated by inductively coupled coils. Moreover, the ICPT method can be divided into the two-coil and four-coil coupling technology. As the name implies, the four-coil ICPT contains two more power-transferring units, which increase the impedance of the system. In other words, the four-coil ICPT receiver side contains two more coils in separate layers[34] compared with the two-coil system. For electronic contact lenses, the two-coil coupling ICPT is generally applied and can achieve flexible adjustment by tuning the coil geometry or matching components to meet the resonant frequency with a high transfer efficiency.[35–37] For electronic contact lens antenna design, the uppermost mission is to transfer power without impeding vision, where the leading component is the pupil unit with a maximum 8 mm diameter. In terms of the antenna shape, single-loop modelling can achieve the expected power transfer in the most concise form, but it normally requires external capacitance to accomplish impedance matching, which largely increases the lens thickness and contains extra components that burden the contact lens. Different antenna shapes on contact lenses vary from dipole antenna to a stretchable S shape.[38] In addition to the impedance-matching issue, the antenna would be bare and coarse on the human eye without a proper encapsulation method. This work presents a self-tuned spiral-shaped antenna for an electronic contact lens. **Table 1** shows a comparison of recent advances in electronic contact lenses. Multiple shapes and geometries have been approached, such as single loop, S shape, dipole, and spiral, to avoid blocking vision. Although the resonant frequency varies from 13.56 MHz to 2.45 GHz, most of the works require extra capacitors for tuning resonant frequency and lacking proper encapsulation, and the S_{11} performance is less satisfactory. However, this work presents a spiral-shaped antenna on an electronic contact lens, which is placed on top of a polyimide layer with an inner diameter of 8 mm and encapsulated with PDMS. Depending on the ambient lighting conditions, the normal pupil size in adults varies from 2 to 8 mm and the amount of light transmitted through the pupil is proportional to its area. Consequently, we believe that such an antenna achieves the required contact lens comfortability without hindering the wearer's vision (Figure 1).

3. Methodology and Embedded Antenna

For a circular spiral antenna, the inductance of the antenna is a vital parameter which mainly relies on the geometry design.

Table 1. A comparison of recent advances in electronic contact lenses.

WPT method	Antenna shape	Working frequency	Matching capacitor [pF]	S_{11} [dB]	Encapsulation	Antenna dimension	Ref.
ICPT	Single-turn loop	925 MHz	50	−13.5	N/A	Coil diameter: 10 mm	[12]
ICPT	Stretchable S shape	551 MHz	1.8	N/A	Parylene-C	Coil diameter: 14 mm Wire width: 70 μm	[31]
ICPT	Spiral windings	13.56 MHz	750	N/A	N/A	Inner diameter: 10 mm Outer diameter: 14 mm	[34]
ICPT	Dipole	850 MHz	N/A	−24	Medical tapes	Arm width: 3 mm Inner diameter: 8 mm	[1]
ICPT	Single loop	13.56 MHz	4700	N/A	N/A	Loop diameter: 12 mm Wire diameter: 0.1 mm	[15]
ICPT	Spiral	2.45 GHz	N/A	−27	PDMS	Inner diameter: 10 mm Outer diameter: 12 mm Wire width: 0.2 mm	This work

As **Figure 2**a shows, the inductance relates to the circular spiral antenna line width, w, fill factor, β, average turn diameter, d_{avg}, and copper magnetic permeability, μ, shown in Equation (1)

$$L_{\text{spiral}} = \frac{\mu N^2 d_{\text{avg}}}{2}\left(\ln\left(\frac{2.46}{\beta}\right) + 0.2\beta^2\right) \tag{1}$$

where $\beta = \frac{d-d_{\text{in}}}{d+d_{\text{in}}}$, $d_{\text{avg}} = \frac{1}{2}(d + d_{\text{in}})$, and $d = d_{\text{in}} + 2Nw + 2(N-1)s$, which predicts the inductance of the antenna by the relationship of these geometry parameters.

Based on Equation (1), a spiral antenna can be designed using Archimedean spiral theory, denoted as Equation (2)

$$r = r_0 + a\phi \tag{2}$$

where r_0 is the starting radius, a is the growth rate of the spiral, and ϕ denotes the angle or the arc value. A circular spiral antenna can be designed in a high-frequency structure simulator (HFSS) by connecting the functionalized curve-based lines, and the function is defined in Equation (3).

$$x_{(t)} = r_0 e^{at}\cos(t) \text{ and } y_{(t)} = r_0 e^{at}\sin(t) \tag{3}$$

From Equation (3), the initial inner circular radius r_0 denotes the starting radius, which is set to 4.8 mm; $a$was set to 10 mm and the rotating end time was set to 6π to ensure the number of turns was 3. The inductive property of the antenna is related to the copper wire width, and the capacitive characteristic is determined by the inner gap distance. Impedance matching is the process of tuning these two parameters. Generally, the resonant frequency has a positive correlation with the copper wire width, and the antenna can achieve a lower frequency, because the start point is closer to the centre point, which would block the wearer's vision. However, this impedance-matching process is nonlinear, as the single variable method is not applicable to this spiral configuration.

The line width of the antenna was set to 0.2 mm for easy fabrication, because, in real condition, there are multiple layers inside human eyes, where different permittivities affect the performance of a contact lens antenna. Thus, in simulation, an eye model was built to imitate the real condition for the human eye, as shown in Figure 2b. The adult eye sphere diameter is normally 24 mm, with three outer layers: the sclera, choroid, and retina. The lens is inside the eye sphere and just behind the cornea, with aqueous humour liquid in between. However, it is formed as a nucleus shape with a former convex curvature $R = 10$ mm, posterior convex curvature $R = 6$ mm, and front-to-rear diameter of 5 mm. When building all those objects, their permeability, conductivity, and density were assigned to imitate the real case at 2.4 GHz, as shown in **Table 2**. Before wrapping the antenna onto the eyeball model, a flat eyeball was designed for better contact between the contact lens and eyeball model, where the cornea and lens part inside the human eye were considered as two cylinders with 7 mm thickness and 5 and 7.5 mm radius, respectively. In addition, the PDMS layer was designed as a cylinder as well on top of the flat eyeball and touched the top surface perfectly.

The contact lens geometry onto the eyeball surface was not achievable by applying a "wrap sheet" function in HFSS because the top layer of the eyeball was not a regular shape. Thus, an object with the outer surface shape of the contact lens was created so that a PDMS (permittivity $\varepsilon_r = 2.5$) layer can be placed to touch the eyeball perfectly. PDMS acted as an encapsulation layer for the contact lens between the coil and the cornea. Polyimide (permittivity $\varepsilon_r = 3.5$, loss tangent tan $\delta = 0.008$) was used as a substrate layer for the antenna. Commercially available contact lenses are often made with highly liquid polyhydroxyethylmethacrylate (HEMA), which provides the ability to conform as a round hemispheroid automatically when it contacts with the eyeball surface. However, fabricating a copper coil on top of materials such as HEMA has been challenging. Instead, polyimide could be a good choice as the substrate for a laboratory-use electronic contact lens. In terms of the actual shape contacting the eyeball, the surface of the eye sphere where the area was exactly as the commercialized contact lens size was detached as the PDMS shape, and a thickness of 100 μm was assigned as the substrate thickness, because it is the best way to imitate the form when it touches perfectly with the eyeball, as shown in Figure 2c.

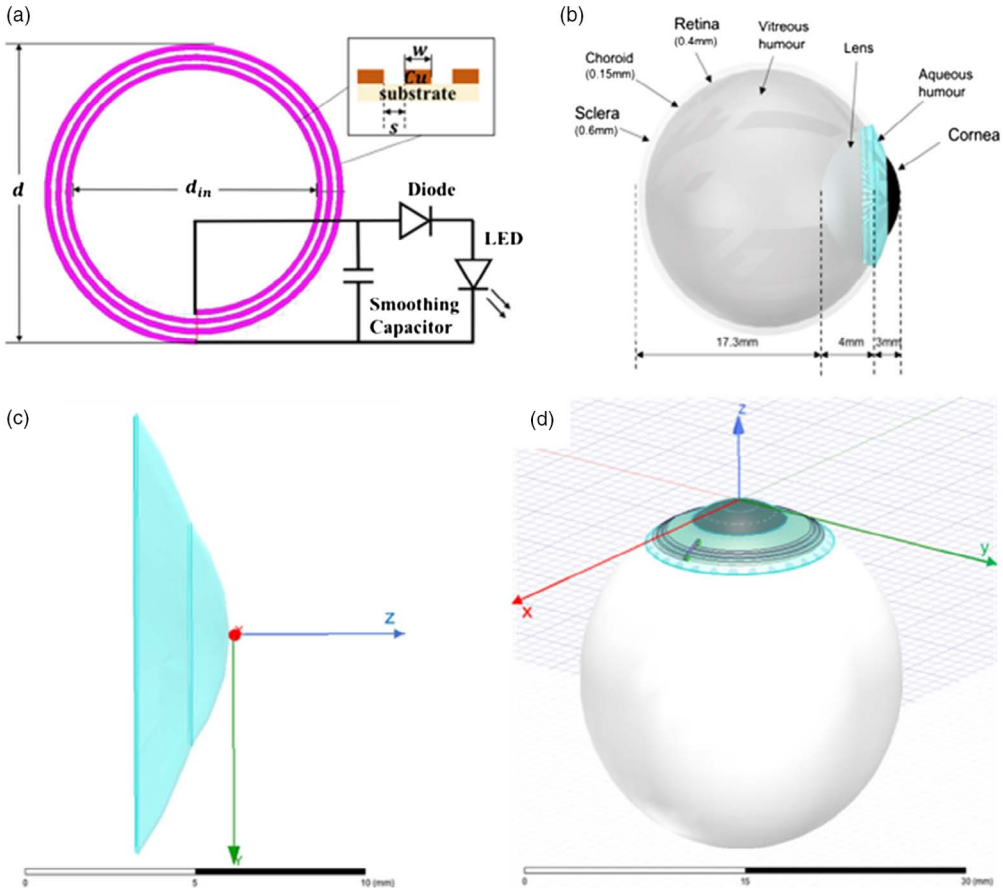

Figure 2. a) Circular spiral antenna design dominating parameters with a rectifying circuit. Geometry of b) eye model, c) PDMS-encapsulated layer, and d) contact lens antenna used for simulations in HFSS.

Table 2. Electromagnetic parameters of eye tissues at 2.4 GHz.

Tissue	Relative permittivity [ϵ_r]	Electrical conductivity σ [S m^{-1}]	Density ρ [kg m^{-3}]
Aqueous humour	66.3	3.41	994
Choroid	58.3	2.50	1050
Cornea	51.7	2.26	1062
Lens	34.0	1.06	1076
Retina	49.0	1.77	1036
Sclera	52.7	2.00	1032
Vitreous humour	68.2	2.44	1005

The "projection tool" in HFSS was used to project the circular coil pattern onto the surface of the eyeball covered by the PDMS layer, as shown in Figure 2d.

4. Fabrication, Moulding, and Encapsulation

The antenna was fabricated on a donut-shaped flexible and biocompatible polyimide substrate (Dupont Pyralux AP 8535R), with a thickness of 0.0762 mm, an internal diameter of 8 mm, and an external diameter of 13 mm. The sizes were chosen according to the human pupil in the iris eye to avoid any obstructing vision. PDMS was used for encapsulation, as it is a highly biocompatible, flexible, and transparent material that is now widely used in the fabrication of contact lenses and embedded medical equipment.[39,40] To encapsulate the antenna with PDMS and give the contact lens shape, a 3D-printed mould was formed. The steps that lead to the contact lens geometry and encapsulation are shown in **Figure 3**. The 3D-printed mould in Figure 3 consists of two parts. The bottom part consists of a base with an inward hemisphere 14 mm in diameter and 2 mm in depth. The upper part is a duplicate, but with the hemisphere outward and 1.5 mm in depth, which is designed to leave 0.5 mm for the contact lens. One of the important steps before encapsulation is PDMS preparation. PDMS elastomer Sylgard 184 was used for encapsulation. Sylgard 184 and a curing agent was mixed in a ratio of 10:1 in a temporary container at room temperature for 5 min to prepare the PDMS.[41,42] A vacuum desiccator was used to degas the solution. Then, PDMS was left to be prepared at room temperature for 10 min. This PDMS was then placed into the bottom mould and subsequently, the fabricated antenna with electronic components was placed into the mould. Finally, the encapsulation and shape of the contact lens

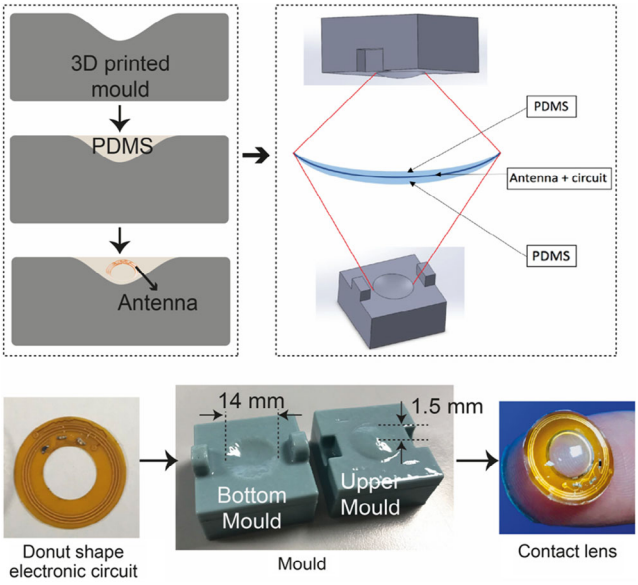

Figure 3. Contact lens mould top and bottom components design, fabrication, and encapsulated electronic contact lens status before and after the 3D-printed mould.

were obtained by squeezing the antenna with the upper mould. After 19 h of heating at 75 °C, the final version of the device was obtained with both sides encapsulated and no bubble inside.[43]

As for lighting a μLED at the load side, a half-wave circuit was fabricated for testing the influence of the electronic components on the antenna performance, where the input signal was a 5 V sinusoidal wave with a Schottky diode, a 1 pF capacitator, and a μLED.

5. Results

Figure 4a shows a schematic diagram of the experimental setup. To accurately mimic the human eye, an ocular imaging eye model (OEMI-7) was used. This model includes natural surfaces of the human eye, including the anterior chamber and crystalline lens. An Agilent E8362B Vector Network Analyzer (VNA) was used to measure the antenna performance (reflection coefficient), which has a frequency range from 10 MHz to 20 GHz. For a projected contact lens antenna, the resonant frequencies are between 2 and 3 GHz, regardless of wire width, gap, or increment. Thus, the expected verified tuning frequency should be 2.45 GHz within 2.4–2.5 GHz, where the antenna can transfer information back and forth in the ISM frequency band.[44] After multiple trials and parameter sweeping, the contact lens antenna on the eyeball was tuned to ≈2.47 GHz resonant frequency.

The fabricated electronic contact lens is shown in Figure 4b. It was tested under three scenarios, as shown in Figure 4d–f. The experimental results were compared with the simulated data shown in **Figure 5**a. Apart from using the OEMI-7 eye model, the reflection coefficient S_{11} of the fabricated antenna was also measured in hand and in saline solution. Generally, the simulated flat version of the contact lens antenna on a hand resonates at 2.45 GHz with S_{11} of −25 dB. In contrast, a curved contact lens antenna on an eye model resonates at a slightly lower frequency. The curved antenna has a minimum of −10 dB bandwidth of 0.7 GHz (2.40–2.47 GHz), thereby covering the entire ISM band. Furthermore, the influence of the other electronic components on the antenna performance was negligible. However, the measured antenna performance in OEMI-7 shifted to a higher frequency, as shown in Figure 5a. This may be caused by the imperfect touch of the antenna with the eye model, which creates an air gap in between. Nonetheless, the ocular imaging eye model OEMI-7 from Ocular Instruments only contains vitreous humour inside, which does not exactly mimic the simulated eyeball condition and which may add to the measurement inaccuracy.[45] Limited by the real case equipment for practical measurement, the performance of the contact lens antenna was measured on hand tissue as well as in saline solution. A comparison among these results indicates that the measurement with hand was the closest to simulation, as shown in Figure 5a. indicating that the contact lens antenna resonates at 2.4 GHz with more than −12 dB return loss. On the other hand, due to higher conductivity (lossy component), the resonant frequency of the contact lens is reduced in saline solution, as shown in Figure 5a.

To demonstrate that the PDMS-encapsulated contact lens does not interfere with transmission of light or vision, different thicknesses of PDMS were chosen for the light absorbance test by using the Ultrospec 9000 spectrophotometer. This is a variable bandwidth, dual-beam UV–vis spectrophotometer, which is European Pharmacopoeia compatible. The different thicknesses of PDMS were obtained using different spin coating speeds (w) while maintaining the spin time (t) as 150 s. The formula for calculating the theoretical thickness is

$$h = \left(\frac{3\mu}{4\rho}\right)\frac{1}{w\sqrt{t}} \tag{4}$$

where h is the thickness of PDMS, μ is the viscosity of the cured PDMS, and ρ is the density of the PDMS.[3,46] Consequently, three different PDMS thicknesses were obtained using coating speeds of 500, 750, and 1000 rpm, respectively. Each PDMS sample was attached to a spectrophotometer cuvette and measured against a reference cuvette. As shown in the absorption spectrum in Figure 5b, there was negligible light absorption in the visible spectrum (≈380–740 nm) for all three tested PDMS thicknesses. This indicates that the PDMS layer was unlikely to impact the quality of vision through the contact lens. It should be noted that the peak below 350 nm in UV absorption was due to the glass support used.

To evaluate the safety of electromagnetic exposure of the contact lens antenna, the specific absorption rate (SAR) distributions near the eye of a realistic human model were calculated using HFSS, as shown in **Figure 6**a. The SAR behavior in the homogeneous human model was evaluated based on the simulation setup in Figure 6b. The contact lens with the antenna was placed touching the eye. The highest SAR value was concentrated in the eye nearest to the contact lens antenna and degraded rapidly toward the back of the eye. For 0.1 W of transmitted power by the antenna, the maximum 1 g average SAR was 0.4 W kg^{-1}. The simulated SAR in HFSS was within the safety standard given by Institute of Electrical and Electronics Engineers (IEEE).

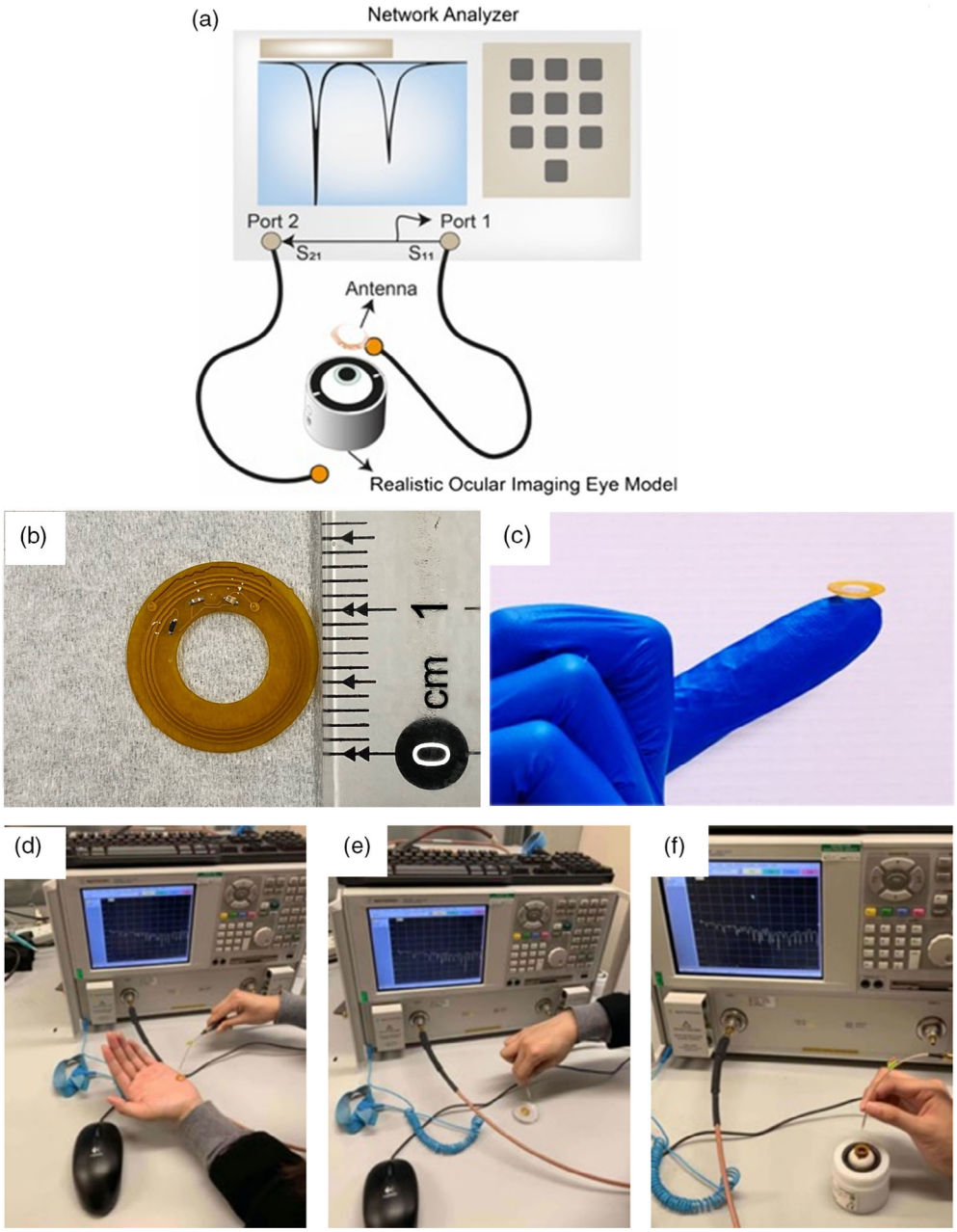

Figure 4. a) A schematic diagram of the experimental setup with a realistic eye model. b) Fabricated contact lens antenna size with a scaling ruler. c) Contact lens antenna curved and encapsulated with PDMS layer. d) Measurement on hand (The experiment has been performed with the full, informed consent of the subject, who is also the first author of the manuscript). e) Measurement on water surface. f) Measurement on eye model.

According to IEEE, the 1 and 10 g SAR is limited to 1.6 and 2 W Kg^{-1}, respectively, for the implantable antenna system.[47] The evaluated transmitted power of 0.1 W was much higher than the required transmitter power (25 μW); therefore, SAR should not be a problem for the proposed electronic contact lens antenna under the IEEE safety regulations.

In addition, the 3D radiation pattern of the electronic contact lens antenna is shown in Figure 6b. The antenna achieves a maximum gain of −28 dBi radiated outward from the contact lens. The obtained gain was more than enough for data communication at a moderate range.[48,49] As a result, the contact lens antenna can also be modified for wireless data communication purposes at 2.45 GHz.

6. Conclusions

In this article, a proof-of-concept electronic contact lens with an integrated antenna, circuits, and μLED was designed, fabricated, and encapsulated with PDMS material. The electronic contact

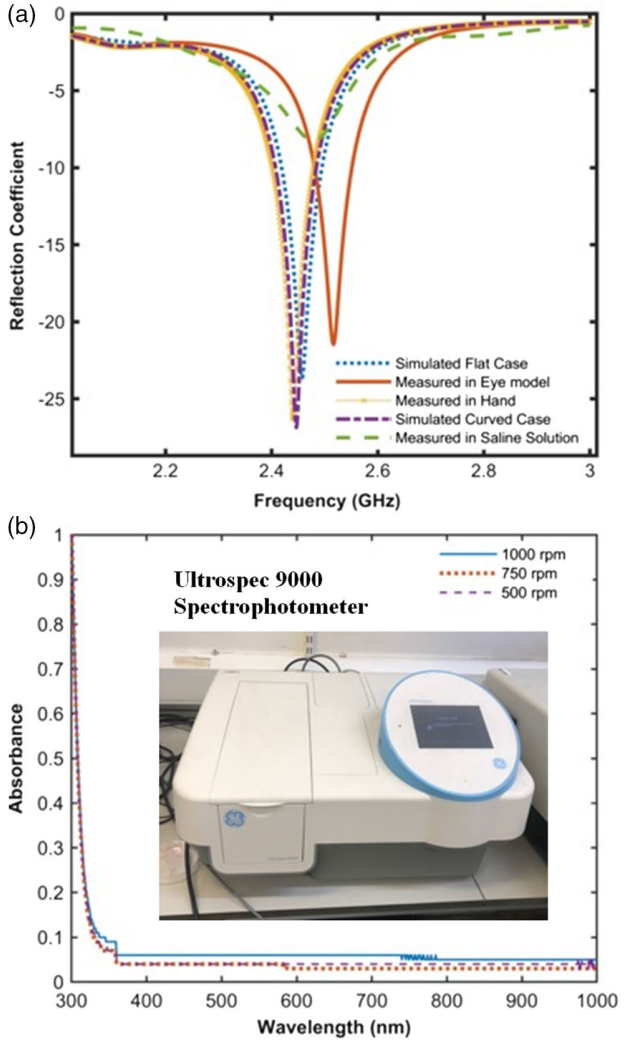

Figure 5. a) Measurement results compared with the simulation results. b) Measurement of transmission of light through different thicknesses of PDMS encapsulation layers using a spectrophotometer.

lens was tested using a realistic eye model. The antenna was tuned in the 2.45 GHz ISM band and the antenna performance was simulated using HFSS. The proposed antenna was self-tuned without additional capacitor or inductor components. Antenna performance was also checked by VNA under different conditions, such as in the palm of a hand, in water, on an eye model, and in saline solution. Our results show that the curved antenna has a −10 dB bandwidth of 0.7 GHz. The maximum antenna gain was −28 dBi and the contact lens also satisfies the electromagnetic exposure safety limit. Different contact lens thicknesses were also tested. Our spectrophotometer results show that the PDMS material thickness is unlikely to impact the quality of vision. There are limitations to this work. For example, we have only used PDMS material. In future, we will extend this work by investigating other materials that are used in contact lenses, such as hydrogels. Moreover, we will investigate methods to simultaneously transfer data and power using in vivo experiments. This will enable us to track the lens' performance in a real-world environment that involves dynamic movements. Therefore, we will be able to follow the current trend of smart contact lenses, which is leaning toward smaller antenna sizes with a high power transfer efficiency. Moreover, these lenses would need to be fabricated using materials that are more compatible with the human body.

Acknowledgements

This work was partially supported by the UK EPSRC under grant EP/R511705/1 and PEER1819/03 from Scottish Research Partnership in Engineering (SRPe).

Conflict of Interest

The authors declare no conflict of interest.

Keywords

electronic contact lenses, remote health monitoring, wearable electronics

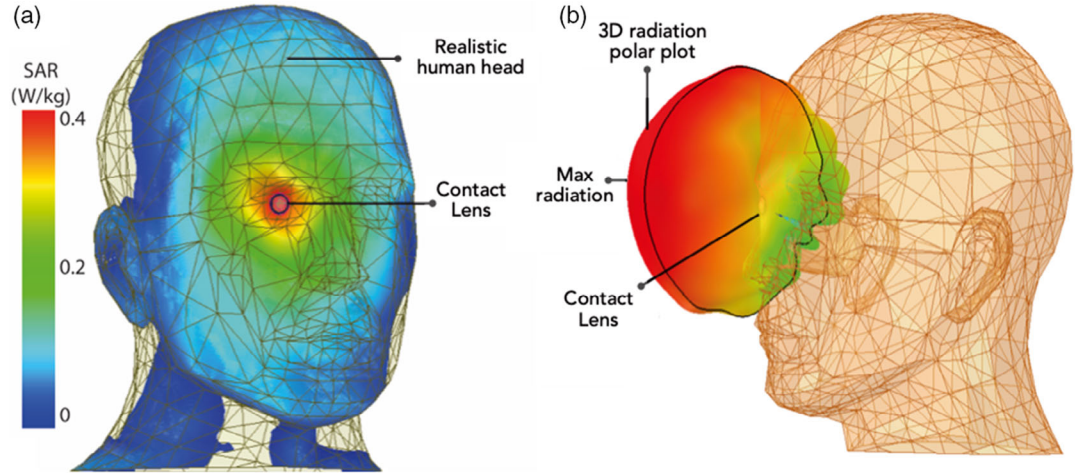

Figure 6. a) SAR distributions near the eye of a realistic human model. b) 3D radiation pattern in Ansys HFSS simulation environment.

Received: December 31, 2019
Revised: February 6, 2020
Published online: February 28, 2020

[1] L. Y. Chen, B. Milligan, T. Qu, L. Jeevananthan, G. Shaker, S. Safavi-Naeini, *IEEE Antennas Propag. Mag.* **2018**, *60*, 108.
[2] J. Kim, M. Kim, M. Lee, K. Kim, S. Ji, Y.-T. Kim, J. Park, K. Na, K.-H. Bae, H. K. Kim, F. Bien, C. Y. Lee, J.-U. Park, *Nat. Commun.* **2017**, *8*, 14997.
[3] J. Park, J. Kim, S. Y. Kim, W. H. Cheong, J. Jang, Y. G. Park, K. Na, Y. T. Kim, J. H. Heo, C. Y. Lee, J. H. Lee, F. Bien, J. U. Park, *Sci. Adv.* **2018**, *4*, eaap9841.
[4] S. Park, D. Y. Lee, *Cutting-Edge Enabling Technol. Regener. Med.* **2018**, *1078*, 155.
[5] C. Song, G. Ben-Shlomo, L. Que, *J. Microelectromech. Syst.* **2019**, *28*, 810.
[6] T. Takamatsu, Y. Chen, T. Yoshimasu, M. Nishizawa, T. Miyake, *Adv. Mater. Technol.* **2019**, *4*, 1800671.
[7] K. Choi, H. G. Park, *ACS Nano* **2017**, *11*, 5223.
[8] S. Lee, I. Jo, S. Kang, B. Jang, J. Moon, J. B. Park, S. Lee, S. Rho, Y. Kim, B. H. Hong, *ACS Nano* **2017**, *11*, 5318.
[9] M. Nasreldin, R. Delattre, M. Ramuz, C. Lahuec, T. Djenizian, J. L. D. de la Tocnaye, *Sensors*, **2019**, *19*, 2062.
[10] D. T. Markus, M. C. Hayes, US Patent App. 14/337,213, **2018**.
[11] L. Y. Chen, G. Shaker, S. Safavi-Naeini, in *IEEE Int. Symp. on Antennas and Propagation and Usnc/Ursi National Radio Science Meeting*, IEEE, Piscataway, NJ **2015**, p. 358.
[12] J. C. Chiou, S. H. Hsu, Y. T. Liao, Y.-C. Huang, G.-T. Yeh, C.-K. Kuei, K.-S. Dai, *IEEE J. Biomed. Health Inf.* **2016**, *20*, 1216.
[13] J. Zhao, R. Ghannam, M. Yuan, H. Tam, M. Imran, H. Heidari, *J. Low Power Electronics* **2019**, *15*, 76.
[14] K. N. Bocan, E. Sejdic, *Sensors* **2016**, *16*, E393.
[15] T. Takamatsu, Y. Sijie, F. Shujie, L. Xiaohan, T. Miyake, in *Advanced Functional Materials*, John Wiley & Sons, Inc., Hoboken, NJ **2019**.
[16] R. Das, Y. Cho, H. Yoo, in *IEEE MTT-S Int. Microwave Symp. (IMS)*, San Francisco, CA **2016**.
[17] M. Schormans, V. Valente, A. Demosthenous, *IEEE Trans. Biomed. Circuits Syst.* **2019**, *13*, 592.
[18] Z. Yang, W. T. Liu, E. Basham, *IEEE Trans. Magn.* **2007**, *43*, 3851.
[19] J. C. Lin, *IEEE Antennas Propag. Mag.* **2006**, *48*, 157.
[20] R. Lingley, M. Ali, Y. Liao, R. Mirjalili, M. Klonner, M. Sopanen, S. Suihkonen, T. Shen, B. P. Otis, H. Lipsanen, B. A. Parviz, *J. Micromech. Microeng.* **2011**, *21*, 125014.
[21] H. Yao, A. J. Shum, M. Cowan, I. Lähdesmäki, B. A. Parviz, *Biosens. Bioelectron.* **2011**, *26*, 3290.
[22] J. C. Chiou, S. H. Hsu, Y. C. Huang, G. T. Yeh, W. T. Liou, C. K. Kuei, *Sensors* **2017**, *17*, 108.
[23] A. Vásquez Quintero, R. Verplancke, H. De Smet, J. Vanfleteren, *Adv. Mater. Technol.* **2017**, *2*, 1700073.
[24] N. M. Farandos, A. K. Yetisen, M. J. Monteiro, C. R. Lowe, S. H. Yun, *Adv. Healthcare Mater.* **2015**, *4*, 792.
[25] A. R. Lingley, B. P. Otis, T. T. Shen, B. A. Parviz, *Microsyst. Technol.* **2012**, *18*, 453.
[26] G. Mattana, T. Kinkeldei, D. Leuenberger, C. Ataman, J. J. Ruan, F. Molina-Lopez, A. V. Quintero, G. Nisato, G. Tröster, D. Briand, N. F. de Rooij, *IEEE Sens. J.* **2013**, *13*, 3901.
[27] R. Narayanamoorthi, *IEEE Trans. Compon. Packag. Manuf. Technol.* **2019**, *9*, 1253.
[28] Y. Liao, H. Yao, A. Lingley, B. Parviz, B. P. Otis, *IEEE J. Solid-State Circuits* **2012**, *47*, 335.
[29] M. Yuan, H. Heidari, *M.Sc. Thesis*, University of Glasgow **2019**.
[30] B. Ng, P. Heckler, A. Do, P. Azar, E. Leon, T. Smilkstein, in *Proc. of IEEE Engineering in Medicine and Biology Conf (EMBC)*, Chicago **2014**, p. 5956.
[31] P. Chen, S. Saati, R. Varma, M. S. Humayun, Y. Tai, in *IEEE Int Conf on Micro Electro Mechanical Systems*, Vol. *87*, Sorrento, Italy **2009**, pp. 244–247.
[32] G. Chen, H. Ghaed, R. Haque, M. Wieckowski, Y. Kim, G. Kim, D. Fick, D. Kim, M. Seok, K. Wise, D. Blaauw, D. Sylvester, *IEEE Int. Solid-State Circuits Conf.*, Vol. *60*, IEEE, Piscataway, NJ **2011**, pp. 310–312.
[33] M. Leonardi, E. M. Pitchon, A. Bertsch, P. Renaud, A. Mermoud, *Acta Ophthalmol.* **2009**, *87*, pp. 433–437.
[34] L. R. Chen, G. Shaker, S. Safavi-Naeini, in *IEEE Int. Symp. Antennas Propagation. Conf.*, IEEE, Piscataway, NJ **2017**, p. 1293.
[35] R. Lockhart, R. Dauksevicius, A. Vasquez Quintero, P. Janphuang, D. Briand, N. F. de Rooij, *J. Phys. Conf. Ser.* **2013**, *476*, 2113.
[36] R. Yin, Z. Xu, M. Mei, Z. Chen, K. Wang, Y. Liu, T. Tang, M. K. Priydarshi, X. Meng, S. Zhao, B. Deng, H. Peng, Z. Liu, X. Duan, *Nat. Commun.* **2018**, *9*, 2334.
[37] K. Mansouri, T. Shaarawy, *Br. J. Ophthalmol.* **2011**, *95*, 627.
[38] M. H. M. Kouhani, A. Weber, W. Li, in *IEEE Int. Conf. Micro Electro Mechanical Systems (MEMS)*, IEEE, Piscataway, NJ **2017**, pp. 557–560.
[39] R. D. Munje, S. Muthukumar, S. Prasada, *Sens. Actuators, B* **2017**, *238*, 482.
[40] S. Kim, J. S. Ho, A. S. Y. Poon, *Phys. Rev. Lett.* **2013**, *110*, 203905.
[41] M. Donora, E. Gonzalez-Fernandez, A. Vásquez Quintero, H. De Smet, I. Underwood, *Sens. Actuators, B* **2019**, *296*, 126671.
[42] N. Fattah, S. Laha, D. Sokolov, G. Chester, P. Degenaar, *IEEE Engineering in Medicine and Biology Society (EMBC). Conf.*, IEEE, Piscataway, NJ **2015**, pp. 8006–8009.
[43] P. Gutruf, V. Krishnamurthi, A. Vázquez-Guardado, Z. Xie, A. Banks, C.-J. Su, Y. Xu, C. R. Haney, E. A. Waters, I. Kandela, S. R. Krishnan, T. Ray, J. P. Leshock, Y. Huang, D. Chanda, J. A. Rogers, *Nat. Electron.* **2018**, *1*, 652.
[44] S. Park, D. S. Brenner, G. Shin, C. D. Morgan, B. A. Copits, H. U. Chung, M. Y. Pullen, K. N. Noh, S. Davidson, S. J. Oh, J. Yoon, K. I. Jang, V. K. Samineni, M. Norman, J. G. Grajales-Reyes, S. K. Vogt, S. S. Sundaram, K. M. Wilson, J. S. Ha, R. Xu, T. Pan, T. I. Kim, Y. Huang, M. C. Montana, J. P. Golden, M. R. Bruchas, R. W. Gereau, J. A. Rogers, *Nat. Biotechnol.* **2015**, *33*, 1280.
[45] M. Donora, A. F. V. Quintero, H. De Smet, I. Underwood, *Sens. Actuators, B* **2019**, *303*, 127203.
[46] R. D. Rivers. M.Sc. Thesis, California Polytechnic State University **2010**.
[47] R. Das, A. Basir, H. Yoo, in *IEEE Transactions on Industrial Electronics*, IEEE, Piscataway, NJ **2018**.
[48] A. Kiourti, K. A. Psathas, K. S. Nikita, *Bioelectromagnetics* **2015**, *35*, 1.
[49] Y. Ling, T. An, L. W. Yap, B. Zhu, S. Gong, W. Cheng, *Adv. Mater.* **2019**, 1904664, https://doi.org/10.1002/adma.201904664.